Instituto Superior Técnico (December 2016)

Extended Abstract to obtain the Master of Science Degree in Integrated Master in Chemical Engineering

Bactericidal effect of silver in cellulose acetate mixed matrix membranes – silver nanoparticles vs silver loaded zeolite

Ana Rita Batista Vilas Boas

Keywords

Cellulose acetate membranes
Nanocomposite membranes
Silver nanoparticles
ZSM-5 zeolite
Antibacterial properties

Abstract

Nanofiltration is still affected by biofouling, which can be minimized using mixed matrix membranes with antibacterial properties. Thus, seven cellulose acetate asymmetric composite membranes were prepared via the wet-phase inversion method incorporating, in the membrane casting solutions, silver nanoparticles, ZSM-5 zeolite and different contents of silver exchanged zeolite (0,005%, 0,03%, 0,07% and 0,14% of silver in the membrane), which compositions were confirmed by thermogravimetric analysis. The silver nanoparticles formation, using silver nitrate, sodium borohydride (reducing agent) and PVP (stabilising agent), can be described by a second order kinetics. The addition of formamide to silver nitrate forms silver particles with different size distributions. It can be stated that silver nanoparticles increase the hydraulic permeability of cellulose acetate membranes, contrary to ZSM-5 zeolite, and the increasing concentration of silver exchanged zeolite increases this parameter. The incorporation of these materials decreases the rejection coefficients to glucose, NaCl, Na_2SO_4, $MgCl_2$ and $MgSO_4$, as the zeta potential of the membranes. The silver present in the zeolite, both in powder and in the membrane, is in the cationic form, as seen in the cyclic voltammetry curves. The silver zeolite membrane (0,14% silver) showed the lowest bacterial growth of *Escherichia coli* and *Pseudomonas aeruginosa* after 300 minutes. The ZSM-5 zeolite had no bactericidal effect against the cultures, contrary to the silver exchanged zeolite that showed higher effect against *E. coli*.

1 INTRODUCTION

Nanofiltration is used in wastewater treatment and drinking/process water production and is the best available technique for removal of natural organic matter (NOM) and to avoid formation of disinfection by-products (DBP), surpassing the traditional methods as a result of the development of the membranes and the better prices due to enhanced use coupled with a more demanding water quality. However, nanofiltration is still hindered by membrane fouling, as it reduces membrane permeability [1–3]. The fouling, caused by membrane surface deposition, is hard to remove even with periodic cleaning, which largely increases maintenance and operating costs. For this reason, the best option is to prevent fouling at its earliest stages [4]. Since membranes can have a wide range of characteristics by changing the material or fabrication process, it is possible to create membranes with fouling resistance, by incorporating materials such as zeolites, and antimicrobial properties, such as silver nanoparticles [1,5]. Silver nanoparticles (AgNP) exhibit strong antimicrobial effect against bacteria, viruses and eukaryotic microorganisms due to the continuous release of a low level of silver ions. This release is a function of the nanoparticle size (smaller particles have a faster release rate), the temperature (higher temperatures accelerate dissolution) and exposure to oxygen, sulphur and light [6,7]. The silver nanoparticles get attached to the cell membrane, penetrating inside the bacteria and attacking the respiratory chain and cell division, which leads to cell death. This effect is enhanced with the release of silver ions in the cells [8]. According to Ouay and Stellacci [9], Ag^+ is the actual antibacterial agent of silver nanoparticles, which act as a silver ions reservoir from where the trapped silver ions are released, although the role of metallic silver nanoparticles cannot be excluded. This oxidation can be due to the presence of dissolved atmospheric oxygen in the colloidal solution. D. Koseoglu-Imer et al. [10] prepared polysulfone membranes with different concentrations of silver nanoparticles (0% – 1 wt.%) and observed the following: after the addition of AgNP there was a change in the surface structure of bare PS membrane; the increasing concentration of AgNP leads to aggregation; hydraulic permeability increases and adsorptive fouling decreases with low concentrations of silver

nanoparticles (up to 0,25 wt.%), comparing with the bare membrane; the growth of bacterial colonies decreased with increasing silver nanoparticles concentration; the ionic silver loss from the composite membranes during pure water filtration was minimal.

The ability to replace atoms *via* ion exchange may imbue the zeolite with alternate charge and structural properties [5]. According to P. Lalueza et al. [11], silver exchanged ZSM-5 zeolite, the most commonly applied zeolite in membranes [5], has higher bactericidal effect comparing with silver nanoparticles, result related with the total amount of ionic silver bioavailable, the oxidation state of the silver species and the particle size of the material. Zeolites are considered an inorganic reservoir for hosting ions that regulate their release, providing a rigid and stable structure [8,12]. The antimicrobial activity of faujasite (FAU) zeolites doped with silver was reported by L. Ferreira [12] using bacteria (*Escherichia coli* and *Bacillus subtilis*) and yeast (*Saccharomyces cerevisiae* and *Candida albicans*). Contrary to the silver exchanged samples, the virgin zeolites did not show microbial inhibitory effects, indicating that this behaviour is due to the presence of silver. The Y FAU zeolite displayed lower minimum inhibitory concentration (MIC) for the bacteria (0,2 mg/mL) compared with X FAU (0,3 mg/mL), which could be explained by the presence of metallic silver in the last zeolite verified by XPS analysis. The effect of the silver zeolites on the yeast cultures were less sensitive than bacteria (1,0 mg/mL), which can be explained by the complex cellular organization of eukaryotic cells and the structure of the cellular wall. Higher bioavailability of cationic silver results in a higher bactericidal action of the silver-carrier material. However, further studies are required to clarify the possible long-term toxic effects of silver [11,13,14].

2 EXPERIMENTAL

2.1 MANUFACTURING OF THE MEMBRANES

2.1.1 PREPARATION OF SILVER NANOPARTICLES

The silver nanoparticles suspension was prepared using PVP from BDH Chemicals (~44.000 g/mol), sodium borohydride ($NaBH_4$) and silver nitrate ($AgNO_3$) from Panreac. All the reagents were used as-received, without further purification.

The silver nanoparticles were prepared *ex-situ* according to the synthesis protocol of Figueiredo et al. [15], by the reduction of silver nitrate with sodium borohydride (Eq. 2.1), using polyvinylpyrrolidone (PVP) as the protecting agent [16].

$$AgNO_3 + NaBH_4 \rightarrow Ag^0 + 0{,}5H_2 + 0{,}5B_2H_6 + NaNO_3 \quad (2.1)$$

The nanoparticle synthesis protocol started with the preparation of an aqueous solution of PVP (0,08 g of PVP in a total volume of 8 mL), followed by the dissolving of 0,4988 g of $AgNO_3$ and 0,03026 g of $NaBH_4$, separately, in a total volume of 4 mL of the PVP solution previously prepared. An Erlenmeyer flask filled with the $AgNO_3$ solution was submerged in an ultrasonic bath, shaken and the $NaBH_4$ was dropwise added to the $AgNO_3$ solution. To obtain a complete dissolution of the chemicals, mechanical agitation and ultrasonic bath were used. The obtained suspension, with a homogeneous greenish brown tone, had to be stored in a fridge without exposure to light.

2.1.2 PREPARATION OF THE ZEOLITE

Zeolites in powder are commercially available; ZSM-5 zeolite (Si/Al=15) was obtained from Zeolyst International. $AgNO_3$ from Panreac was used in the ion exchange and NaCl from VWR was used in the titration of the zeolite. All the reagents were used as-received, without further purification.

To load the zeolite with silver, a 0,1 M $AgNO_3$ aqueous solution (400 mL) was prepared and mixed with the zeolite (20 g) during three days with a magnetic stirrer at 600 rpm and without exposure to light to avoid silver reduction. After the exchange, the suspension was filtrated and purged with deionized water. The quantity of silver present in all the solutions was measured by titration after Mohr's method [17], leading to the silver content in the zeolite after the exchange (4,85 wt.%) by the difference between the content in the mother solution (10,5 mmol/L) and in both filtrate (76,0 mmol/L) and purging water (0,7 mmol/L), assuming all silver ions were either in the zeolite or in the filtrate and purging water. The silver loaded zeolite was dried under vacuum and then in a drying oven at 140℃ for 24 hours. Both zeolites, with and without silver, were at last calcined at 500℃ for 24 hours in a muffle furnace.

2.1.3 PREPARATION OF THE CASTING SOLUTIONS

The casting solutions were prepared using cellulose acetate (CA) from Sigma-Aldrich (~30.000 g/mol), acetone from LabChem and formamide from Sigma Aldrich. All the reagents were used as-received, without further purification.

To manufacture the membranes, it was necessary to prepare a casting solution, consisting of a polymer (CA), a solvent system (acetone and formamide) and incorporating materials. The addition sequence was cellulose acetate (17 wt.%), formamide (30 wt.%) and acetone (53 wt.%). For the silver nanoparticles membrane, the respective suspension was added to the acetone in a flask, homogenised and then poured into the bottle with the cellulose acetate and formamide. In the membranes with zeolite, this one was added after the polymer. The flasks were covered with duct tape to avoid acetone evaporation and the ones containing silver were protected from light with aluminium foil. The solutions were mixed in a bottle and agitated until CA was completely dissolved in a P Selecta Vibromatic mechanical agitator at 550 rpm.

2.1.4 CASTING OF THE MEMBRANES

To cast the membranes it was necessary to have a glass plate with a smooth surface without imperfections, a casting knife and a coagulation bath, composed of deionized water and ice. This knife has a groove of 0,25 mm on one side which is responsible

for casting a membrane with the required thickness. The casting solution was poured equally into the slot of the casting knife and the 30 seconds of evaporation time began. The knife, placed with the groove faced down and to the upper part of the glass, was moved through it up to the end, spreading out the casting solution evenly. To assure a uniform membrane, both the glass and the casting knife had to be clean and dry. After the evaporation time, the plate with the casting solution was immersed in the coagulation bath at 0ºC. When the membrane detached from the plate, it was identified on the active layer and stored in the fridge immersed in deionized water in a hermetic box. The asymmetric cellulose acetate and mixed matrix membranes – CA/silver nanoparticles, CA/ZSM-5 zeolite and CA/silver loaded zeolite (with different silver concentrations in the membrane) – were designated as CA400-30 (CA), CA400-30Ag0,14 (CA/Ag0,14), CA400-30ZSM5 (CA/ZSM-5) and CA400-30ZAg0,005 (CA/ZAg0,005), CA400-30ZAg0,03 (CA/ZAg0,03), CA400-30ZAg0,07 (CA/ZAg0,07), CA400-30ZAg0,14 (CA/ZAg0,14), respectively. It was difficult to cast the membranes with higher concentrations of silver containing zeolite (CA400-30ZAg0,14) since the zeolite agglomerates ripped the membrane during the casting.

2.1.5 Annealing treatment

The casted membranes have a pore diameter characteristic of ultrafiltration. An annealing treatment was performed to contract the pores and obtain nanofiltration membranes. It consists of a heat treatment, in which the membranes, inside two petri dishes filled with deionized water, were placed in a thermic bath at 95ºC ± 1ºC for 11 minutes [18]. The membranes used in the bactericidal studies and a silver loaded zeolite membrane (CA400-30ZAg0,14$_P$) were annealed in a heating plate, inside a measurement beaker, at 95ºC ± 2ºC for 11 minutes.

2.2 Evaluation of the permeation performance

2.2.1 Set-up

The characterization of the membranes was made in two crossflow filtration installations, composed of a feed tank, a pump, a flowmeter, two manometers, permeation cells in row and a pressure valve [19]. The flat plate cells have two detachable parts separated by a porous plate (membrane support) with a permeation area of 13,2 cm^2. To avoid damaging the membrane during the experiments, a circular filter paper was placed between the porous plate and the membrane. In the pressurized upper part of the cell, the feed inlet enters and, due to its conical geometry specially designed to achieve a high degree of turbulence, passes tangentially through the membrane, exiting as concentrate [20].

2.2.2 Compaction of the membranes

To avoid fluctuations in the permeation experiments, the membranes had to be compacted for two hours at a pressure approximately 20% higher than the maximum operating pressure (40 bar and 6 bar at the nanofiltration and ultrafiltration installations, respectively) [21].

2.2.3 Hydraulic Permeability

The hydraulic permeability was measured with nanofiltration and ultrafiltration membranes. In nanofiltration conditions, the fluxes were obtained at 5, 10, 15, 20, 25, 30, 35 and 40 bar, with a 0,6 L/min feed flow rate [21]. At the ultrafiltration installation, the fluxes were measured at a feed flow rate of 180 L/h at 1, 2, 3, 4 and 5 bar.

2.2.4 Rejection Coefficients to Solutes

In order to characterize the membranes in terms of rejection coefficient, five solutions were prepared using glucose (Scharlau), NaCl (VWR), Na_2SO_4 (Scharlau), $MgCl_2$ (Riedel-de Haën) and $MgSO_4$ (Merck). The solutions had an initial feed concentration of 2 g/L and samples were taken from permeates and feed (average of feed values before and after the experiment assumed as the bulk feed concentration). The experiment in nanofiltration conditions was conducted at 30 bar and 0,6 L/min, while in ultrafiltration was at 3 bar and 180 L/min. The collected samples were analysed by conductivity measurement for the salts in a Crison Conductimeter GLP 32 and by total organic carbon (TOC) measurement for glucose in a Shimadzu Total Organic Carbon Analyser TOC-V_{CSH}, after obtaining a calibration curve for each compound. The conductivity of the water used to prepare both standard solutions and the ones used in the experiments was lower than 10 μS/cm and was measured with the same conductivity meter. The TOC values were measured as total carbon since inorganic carbon was previously eliminated by acidifying the samples with 10 μL of concentrated sulfuric acid to a pH lower than 2 and shaking them to purge the volatile organic carbon [22]. A dilution was made (1:10) to avoid high carbon concentrations and corrosive effect from a low pH solution. The temperature of the equipment furnace was at 680ºC and the reconstituted air pressure at 200 kPa [23]. At the end of each experiment, the installations were purged with deionized water for 10 minutes at high flows and low pressures [21].

2.3 Characterization

2.3.1 UV-Vis Spectroscopy

In order to characterize the formation of silver nanoparticles and to conclude about formamide use as a reducing agent, the spectra were obtained in a UV-Vis spectrophotometer with diode array detector coupled to a DH-2000-BAL UV-VIS-NIR light source from Micropack and Spectra Suite software. Deionized water was used as the reference sample to take the blank spectrum for all measurements. To conclude about the state of silver particles, three spectra were acquired 30 minutes, three days and four months after the silver nanoparticles preparation. To capture the formation of the silver nanoparticles suspension,

in the 1 mL spectrophotometer cell, 10 μL of the $NaBH_4$ solution (0,02 mol/L) were added to 700 μL of the $AgNO_3$ solution (0,06 mol/L) (to note that both compounds were dissolved in an aqueous solution of PVP), homogenized with a magnetic stirrer. From the variation of maximum absorbance with time it was possible to obtain the kinetics of the silver nanoparticles formation. The effect of the addition of 10 μL of formamide to 500 μL of the $AgNO_3$ solution (solution used in the formation of the silver nanoparticles, 0,06 mol/L) was also monitored in the UV-Vis spectrophotometer.

2.3.2 Electrochemical studies

Cyclic voltammetry (CV) was used to investigate the electrochemical behaviour of the silver inside the porous structure of the zeolite. The electrode consisted in a mixture of zeolite with graphite powder, in a 2:1 (w/w) proportion, a membrane or a membrane placed between two layers of conductive powder. The membranes were cut in the pellet press assembly layout by inserting the membrane in the chamber and pressing it with the piston. The homogenised pellets, which weighted around 5,5 mg, were prepared by simple mixture and subjected to a total applied pressure of 0,5 tonnes during 10 minutes in a PIKE CrushIR hydraulic press. The pellets were then placed in a three-electrode cell, in contact with a platinum auxiliary electrode disc, filled with 5 mL of 0,2 M electrolyte solution of optical grade NaCl (99,99%, Aldrich), and the potentials measured using a silver reference electrode in a Luggin tube [24]. The electrochemical studies were carried out in a Radiometer/Copenhagen DEA101 digital electrochemical analyser, coupled to an IMT102 electrochemical interface, controlled by a computer, which also acquired the data. The results obtained using the membrane/graphite pellets were not reproducible and conclusive.

2.3.3 Thermogravimetric analysis

The thermogravimetric analysis (TGA), used to indirectly characterize the composition of the membranes, was performed in a PerkinElmer STA 6000 coupled to a Pyris Software and a F12-ED Refrigerated/Heating Circulator from Julabo. The membranes were cut in small pieces with a total approximate weight of 20 mg, accommodated in a ceramic pan and then placed over the precision balance. For the sample atmosphere, air was used as the oxidative gas, with a purge rate of 20 mL/minute. The defined temperature scanning programme was the following: hold for 10 min at 30℃, heat from 30℃ to 110℃ at 10℃/min, hold for 15 min at 110℃, heat from 110℃ to 800℃ at 10℃/min, hold for 10 min at 800℃ and cool from 800℃ to 30℃ at 50℃/min [25]. The CA400-30 membrane was considered as the reference value for weight loss.

2.3.4 Determination of the zeta potential

The surface charge properties of a membrane used in aqueous applications strongly influence fouling processes and retention capacity and can be described measuring zeta potential [4]. This technique is influenced by surface composition, pH, nature of ions and ionic strength [26]. This method can also be used to determine the extent and efficiency of chemical modification, such as silver exchanged zeolite [27]. To characterize the zeta potential, an EKA electro kinetic analyser from Anton Paar, coupled with a rectangular cell, Ag/AgCl electrodes and a control and evaluation software (VisioLab for EKA) was used. Two membranes were put into the cell together, with the active layer facing each other, sealed and separated by polytetrafluoroethylene (PTFE) foils. The measurements were carried out with an electrolyte solution of KCl 0,001 M and the pH, varied between 4 and 9, was adjusted with NaOH and HCl 0,1 M. The cell and the bypass were at first rinsed for 60 and 30 seconds, respectively, at 300 mbar. To induce flow two cycles of pressure ramping in each direction were conducted, raising the pressure from 0 to 500 mbar in 120 seconds. The surface conductivity correction was made filling the system with 0,1M KCl [28].

2.4 Evaluation of the bactericidal properties

To assess the bactericidal effect of the seven prepared membranes, the behaviour of two different bacteria cultures (*Escherichia coli* (*E. coli*) and *Pseudomonas aeruginosa* (*P. aeruginosa*)) in the presence of each membrane was evaluated. The cultures were grown in Bacto™ Tryptic Soy Broth (TSB) liquid medium. An optical density around 0,12 at 600 nm read in the spectrophotometer (TSB as the blank) was recommended.

Each side of the annealed membranes, placed in a sterilized petri dish with sterilized water, was sterilized with UV radiation in a laminar flow biological safety cabinet for 30 minutes in order to inactivate microorganisms. After reading the optical density, 1 mL of the inoculum and 9 mL of sterilized water were placed in a 100 mL sterile cup. After taking a blank sample, each membrane was added to *E. coli* and *P. aeruginosa* cultures and shacked in an incubator at 37℃ and 180 rpm. After 18 hours the last sample was collected. To determine bactericidal effect, 100 μL of each culture was taken, approximately every 15 minutes, dilutions were made and spread on Difco™ Tryptic Soy Agar (TSA). The first experiment with *P. aeruginosa* was made during approximately three hours and the second experiment with *E. coli* and *P. aeruginosa* during approximately five hours. The plates were incubated for 24 hours at 37℃ and the number of colonies enumerated in Quebec colony counter.

The number of colonies was expressed in percentage colony forming units (%CFU), given by the Eq. 2.2, to easily compare the results of the different membranes in both cultures, since the initial number of bacteria cells in each experiment was different.

$$\%CFU = \frac{\#colonies_t}{\#colonies_{t=0}} \times 100\% \qquad (2.2)$$

To evaluate the growth of the cultures in the presence of ZSM-5 zeolite and silver containing zeolite, 33,3 μL of *E. coli* and *P.*

aeruginosa cultures were placed in a petri dish with TSA in each part. In the experiment it was used zeolite, with and without silver, sterilized in two different ways: autoclave and by UV radiation. The zeolite was spread in two parts of the petri dish, the remaining being the blank. The plates were incubated for 24 hours at 37℃. The results consisted in the evaluation of bacterial growth in the presence of ZSM-5 zeolite/ZAg, compared to the blank sample.

3 RESULTS AND DISCUSSION

3.1 Hydraulic Permeability

The hydraulic permeability coefficient (L_p) was determined for ultra and nanofiltration membranes (Figure 3-1 and Figure 3-2, respectively). It can be stated that it is influenced by the incorporation of materials.

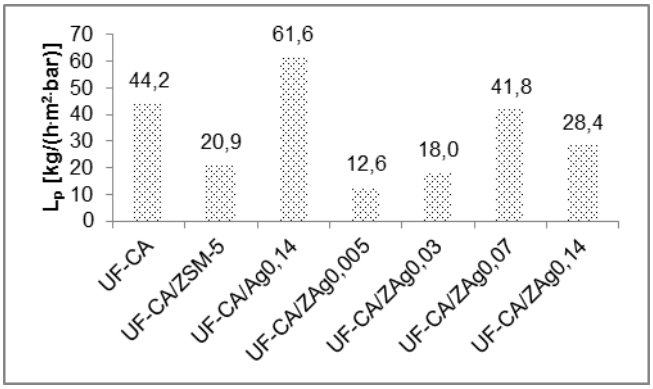

Figure 3-1 – Comparison of the hydraulic permeability of the ultrafiltration membranes.

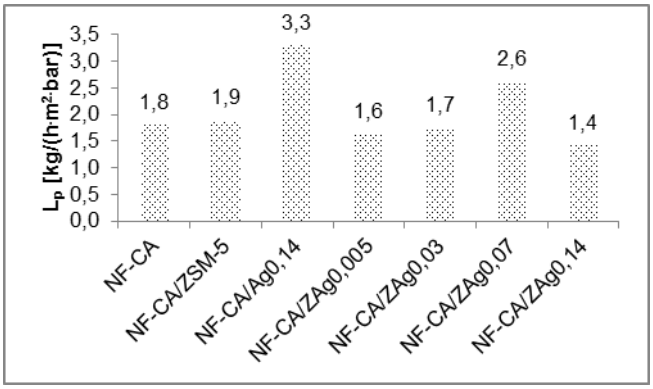

Figure 3-2 – Comparison of the hydraulic permeability of the nanofiltration membranes.

The incorporation of silver nanoparticles increases the hydraulic permeability in comparison with the cellulose acetate membrane (39,6% for UF and 83,1% for NF). This can be explained by the fact that silver nanoparticles prepared *ex-situ* are preferentially located in the skin layer of the membrane and are hydrophilic [29]. The hydraulic permeability of the incorporated ZSM-5 zeolite membrane decreases 52,6% in ultrafiltration conditions, which can be attributed to the hydrophobicity of the ZSM-5 zeolite [30] and the macrovoids reduction [5], and increases 4,5% in nanofiltration conditions, comparing with the CA membrane. The addition of silver loaded zeolite also decreases the hydraulic permeability, which becomes higher with increasing concentration. The CA400-30ZAg0,14 membrane does not follow this trend, probably indicating the existence of a maximum silver zeolite concentration from which the hydraulic permeability decreases [10]. The hydraulic permeability of the NFCA400-30ZAg0,14$_P$ membrane, annealed in a heating plate, was 0,2 kg/(h·m^2·bar), 85,7% lower than the NFCA400-30ZAg0,14 membrane. This is due to the high dependency of hydraulic permeability of CA-400 membranes with temperature: a higher annealing temperature leads to a decrease on hydraulic permeability [18].

3.2 Rejection Coefficient to Solutes

The rejection coefficient was obtained for NaCl, Na_2SO_4, $MgCl_2$, $MgSO_4$ and glucose for ultrafiltration and nanofiltration membranes (Figure 3-3 and Figure 3-4, respectively).

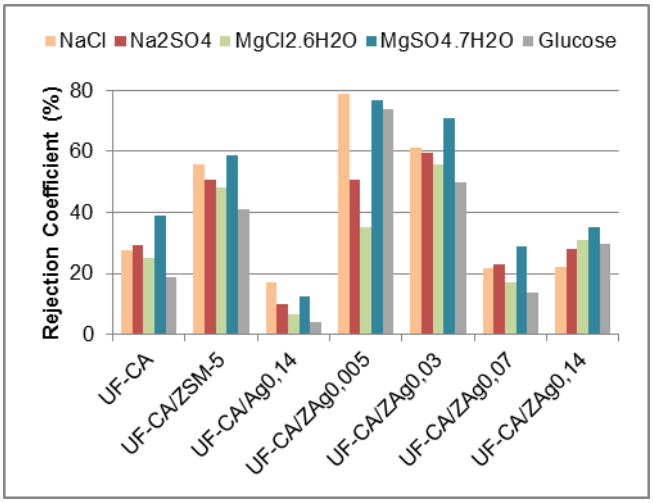

Figure 3-3 – Rejection coefficients for NaCl, Na_2SO_4, $MgCl_2$, $MgSO_4$ and glucose for ultrafiltration membranes.

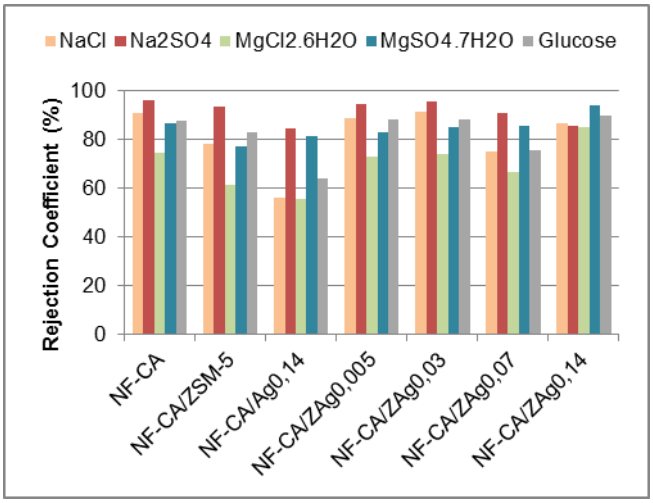

Figure 3-4 – Rejection coefficients for NaCl, Na_2SO_4, $MgCl_2$, $MgSO_4$ and glucose for nanofiltration membranes.

The CA400-30Ag0,14 has rejection coefficients for the salts and glucose lower than the cellulose acetate membrane. The addition of ZSM-5 zeolite increases the rejection coefficients of the UF membrane, in contrast with the NF membrane (slight decrease). In general, the increasing concentration of silver loaded zeolite in the membrane decreases the rejection coefficient. These results are inversely proportional to the obtained for the hydraulic permeability. In nanofiltration

conditions, the rejection coefficients are higher for the Na_2SO_4 salt, which is related with the negative charge of the membrane surface and the higher/lower charge density of the anion/cation [21]. The NFCA400-30ZAg0,14$_P$ membrane had rejection coefficients higher than the ones of the NFCA400-30ZAg0,14 membrane, which annealing was performed in a thermic bath [18].

3.3 UV-Vis Spectroscopy

The three UV absorption spectra of the silver nanoparticles suspension, normalized by peak, at different time periods, are presented in Figure 3-5. As the spectra exhibit a single band with peaks in the typical absorption band range (around 400 nm) and have no visible peak at 600 nm, it can be stated that the prepared suspension has well-dispersed spherical silver nanoparticles [31]. However, the red shift of the maximum absorption from 401 nm in day 1, to 402 nm in day 4 and to 413 nm in day 120 with the bandwidth increase with time indicates an increase in the particle size and a possible aggregation [32]. The diameter of the silver nanoparticles, according to the obtained spectrum in day 1, is 3,2 nm $\pm$ 0,2 nm [31,33].

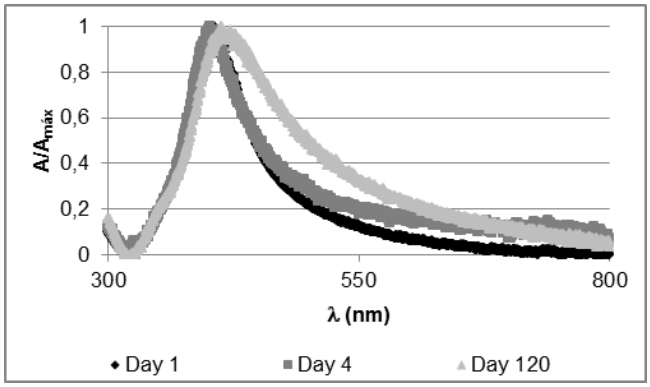

Figure 3-5 – UV absorption spectra normalized by peak of silver nanoparticles suspension at different time periods.

The formation of the silver nanoparticles and the effect of maturing time at initial concentration of 0,01 mL of reducing agent $NaBH_4$, present in Figure 3-6, exhibits absorption peaks around 400 nm, with an increasing absorbance with time (between 0 and 1,4).

From the variation of maximum absorbance with time it was possible to obtain first and second order kinetics of the formation of silver nanoparticles, given by Eq. 3.1 and Eq. 3.2, respectively.

$$A(t) = 1{,}34(1 - e^{-2{,}09t}) \quad (3.1)$$

$$A(t) = 1{,}49 - \frac{1}{1{,}87t + 0{,}67} \quad (3.2)$$

As it can be seen in Figure 3-7, the second order kinetics of the silver nanoparticles formation has the best fitting to the experimental points, with 0,02 as residue sum. The first order kinetics has a residue sum of 0,07.

The effect of the addition of formamide to an aqueous solution of $AgNO_3$ solution is presented in Figure 3-8. The addition of formamide leads to the appearance of a broad extinction band, which can indicate the presence of different distributions of particles sizes: at lower wavelength, well-dispersed spherical nanoparticles and, at longer wavelength, aggregates of primary particles interacting collectively with the incident light as a large silver particle [31,34].

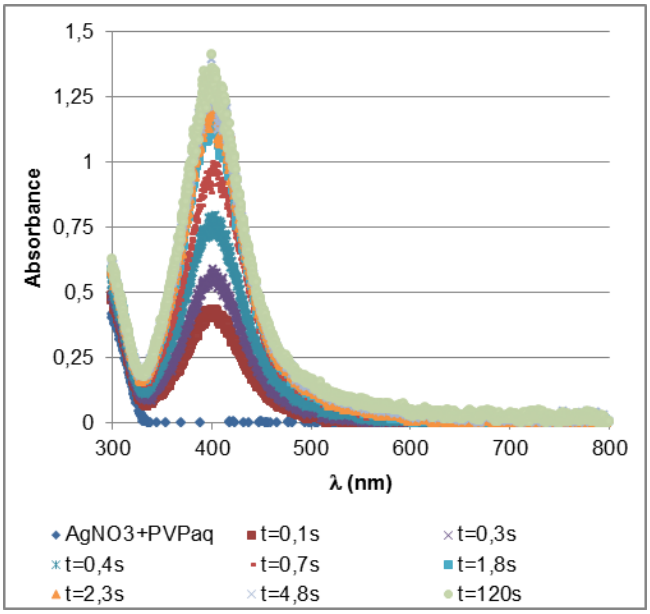

Figure 3-6 – Effect of maturing time at initial concentration of 0,01 mL of reducing agent $NaBH_4$.

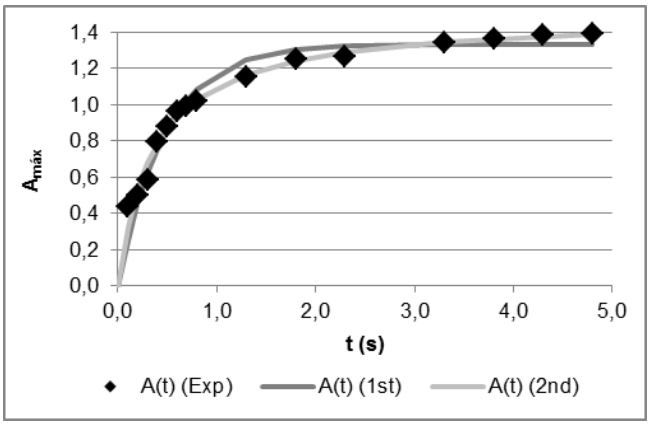

Figure 3-7 – Variation of maximum absorbance with time in the formation of silver nanoparticles.

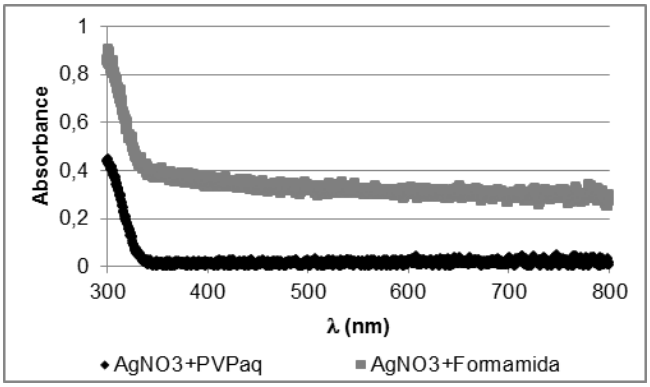

Figure 3-8 – UV absorption spectra of formamide addition to an aqueous solution of $AgNO_3$ (dissolved with PVP).

3.4 Electrochemical studies

3.4.1 Zeolite/Graphite Pellet

The voltammogram of the ZSM-5 zeolite has an irreversible reduction peak at -450 mV in the first cycle (Figure 3-9) that does not appear in the second cycle, which may correspond to a species adsorbed. The voltammograms of the silver exchanged zeolite, starting towards negative potentials (Figure 3-9), show a reduction peak at around -750 mV and in the reverse cycle an oxidation peak around 250 mV. Comparing both CV curves for zeolite and silver loaded zeolite, it can be stated that the peaks appearing in the voltammogram of the silver exchanged zeolite are caused by the silver. The voltammograms of the silver exchanged zeolite, starting with the oxidation scan (Figure 3-10), show a reduction peak at 0 mV and the consequent oxidation at 450 mV, indicating the absence of metallic silver. Thus, the silver exchanged zeolite is present in the cationic form.

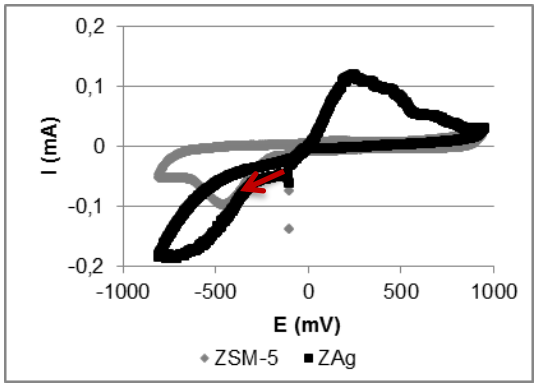

Figure 3-9 – Cyclic voltammograms of calcined ZSM-5 zeolite and silver exchanged zeolite (initial scan towards negative potentials: -100mV → -800mV → 950mV → -100mV, scan rate: 10 mV/s, 1st cycle).

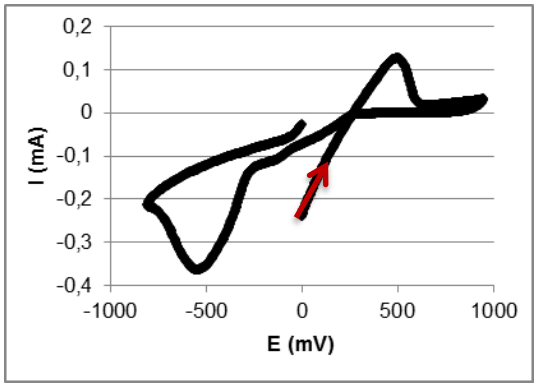

Figure 3-10 – Cyclic voltammogram of calcined silver exchanged zeolite (initial scan towards positive potentials: 0mV → 950mV → -800mV → 0mV, scan rate: 10 mV/s, 1st cycle).

The cyclic voltammetry curves of the pellets with zeolite recovered from the casting solution of CA400-30ZAg0,03 membrane presents differences in the experiments. It may be due to the lack of uniformity of the starting material since it has undergone various washes and possible reactions with the solvents used (formamide and acetone). It can be stated from the CV curves starting towards positive potentials that the silver is in the cationic form since it has no oxidation peak, as in the calcined silver exchanged zeolite. The pellets were made from the same initial sample of graphite/zeolite.

In order to evaluate if a silver ion exchange between the pellet and the electrolyte solution occurs, a silver loaded zeolite/graphite pellet was left in the cell during 74 hours after been subject to six cyclic voltammetry cycles, ensuring that the CV curves obtained were reproducible (Figure 3-11), followed by an oxidation cycle, to guaranty that the silver stayed in the oxidized state. The first and last obtained voltammograms of the oxidized pellet are presented in Figure 3-12.

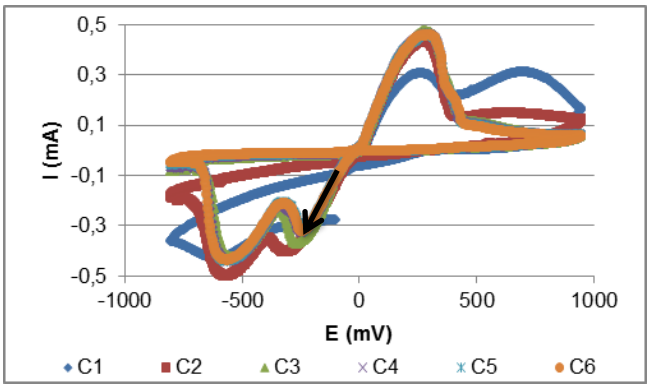

Figure 3-11 – Six sequential cyclic voltammograms of calcined silver exchanged zeolite (initial scan towards negative potentials: -100mV → -800mV → 950mV → -100mV, scan rate: 10 mV/s).

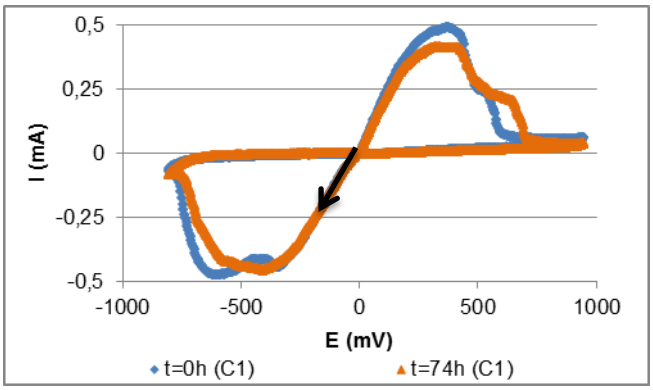

Figure 3-12 – Time evolution of the cyclic voltammograms of calcined silver loaded zeolite to assess the silver ion leaching (initial scan towards negative potentials: 0mV → -800mV → 950mV → 0mV, scan rate: 10 mV/s).

In Figure 3-11, the reduction zone of the first cycle has a broad peak that converts into two well defined peaks in the following cycles, instead of what is observed in the oxidation zone. To compare the cyclic voltammograms (Figure 3-12), an integration of the electric current over time was made for reduction and oxidation peaks, revealing similar values (respectively, 19,8 mC and 16,9 mC at t=0h and 23,5 mC and 21,4 mC at t=74h). It is visible a change of the oxidation pattern with the appearance of an oxidation peak at higher potentials, as the potential was cycled repetitively, which may be due to the diffusion of silver ions into more stable sites in the zeolite, resulting in the slightly shift of the peak potentials towards more positive values [35].

3.4.2 MEMBRANES

Comparing the experiments with the active face of the membrane facing the electrolyte and the electrode, it was decided the first option would be evaluated for being similar to the experiments with the silver containing zeolite. The voltammogram of the UFCA400-30ZAg0,07 membrane starting towards positive potentials (Figure 3-14) shows no oxidation peak, which indicates the absence of metallic silver. Starting towards negative potentials (Figure 3-13), two reduction peaks appear, at -180 mV and -560 mV. The integration of the electric current over time between -100 mV and -700 mV lead to an electric charge of the reduction peaks of 0,2 mC, which corresponds to a silver mass of 0,0002 mg. The UFCA400-30ZAg0,07 membrane, with 0,07% of silver, weighted 1,0 mg and, accordingly, contained 0,0007 mg of silver. Taking into account the uncertainties of the two measurements, the results are comparable.

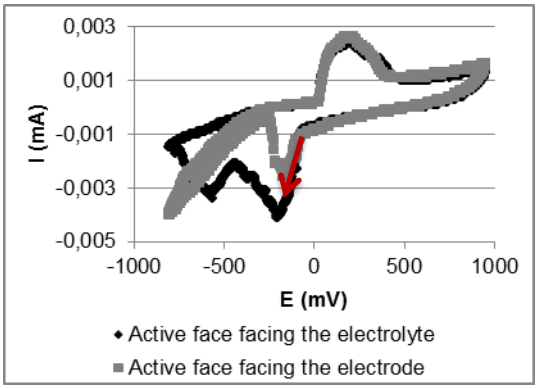

Figure 3-13 – Cyclic voltammograms of UFCA400-30ZAg0,07 membrane, active face facing the electrolyte and the electrode (initial scan towards negative potentials: -100mV → -800mV → 950mV → -100mV, scan rate: 10 mV/s, 1st cycle).

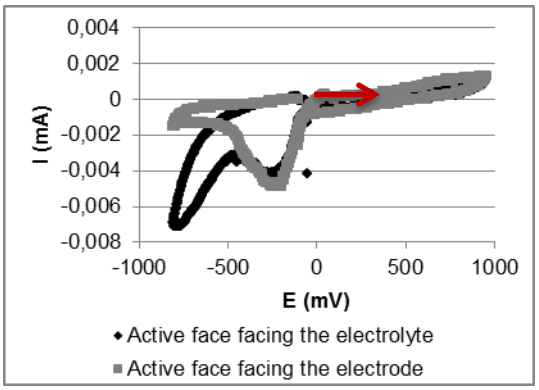

Figure 3-14 – Cyclic voltammograms of UFCA400-30ZAg0,07 membrane, active face facing the electrolyte and the electrode (initial scan towards positive potentials: -100mV → 950mV → -800mV → -100mV, scan rate: 10 mV/s, 1st cycle).

It was not possible to perform more experiments using this method since there was adsorption of silver by the electrode, affecting the following results.

3.5 THERMOGRAVIMETRIC ANALYSIS

In the TGA programme, the weight and heat flow changes as a function of time were obtained: in Figure 3-15, the descending TG curve indicates a weight loss; in Figure 3-16, a positive peak indicates an endothermic process while a negative one indicates an exothermic process. There are two distinct steps: the first one corresponds to the water loss and the second to the cellulose acetate combustion. The dehydration of the membrane starts immediately and stops before the second isothermal step (110℃); the cellulose acetate combustion happens in the second heating ramp, between 350℃ and 600℃. The membranes have around 79% of non-structural water. The final weight obtained for each membrane was the following: 0 mg for UFCA400-30, 0,0462 mg for UFCA400-30Ag0,14, 0,8266 mg for UFCA400-30ZSM5, 0,0030 mg for UFCA400-30ZAg0,005, 0,1239 mg for UFCA400-30ZAg0,03, 0,2229 mg for UFCA400-30ZAg0,07 and 0,5629 mg for UFCA400-30ZAg0,14. The final weight indicates the presence in the membranes of the incorporated materials. In general the obtained results are similar to the expected by the weight percentage in the casting solutions and the different final weight in the second experiment with UF-CA/ZAg0,005 (0,2517 mg) shows that the incorporated components may not be homogeneously dispersed in the membrane.

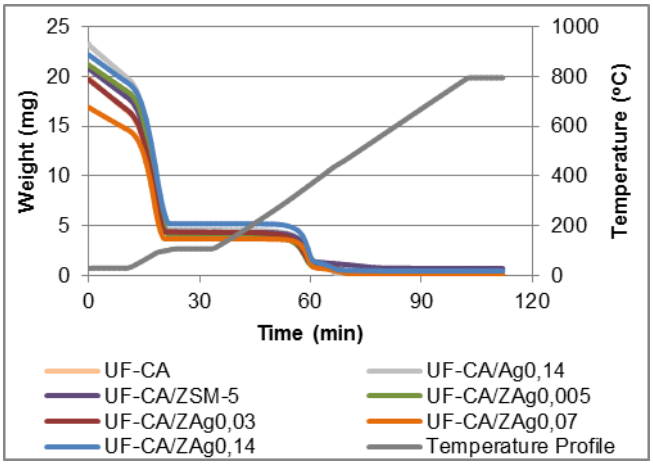

Figure 3-15 – TG curve (weight as a function of time) of the seven prepared membranes.

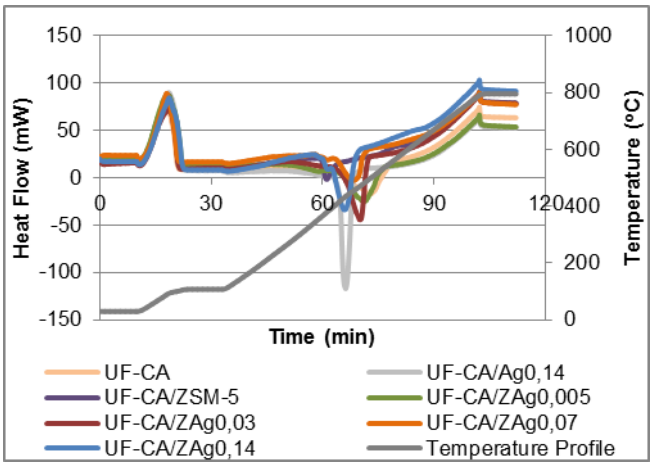

Figure 3-16 – TG curve (heat flow as a function of time) of the seven prepared membranes.

3.6 DETERMINATION OF THE ZETA POTENTIAL

The obtained results (Figure 3-17) show a variation of zeta potential with pH: with increasing pH, zeta potential decreases,

becoming more negative, which is typical of NF cellulose acetate membranes, due to the negatively charge surface [36]. The dependence of zeta potential with pH is different for each membrane, being the NFCA400-30ZAg0,14 membrane the least influenced by the pH. Approximately from pH 6 it is visible a zeta potential stabilization, with a maximum variation of 1,2 mV. The zeta potential of the modified membranes decreases relatively to the NFCA400-30 membrane. The less modified membrane (NFCA400-30ZAg0,005) has the lowest zeta potential, as reported by J. Abitoye et al. [36].

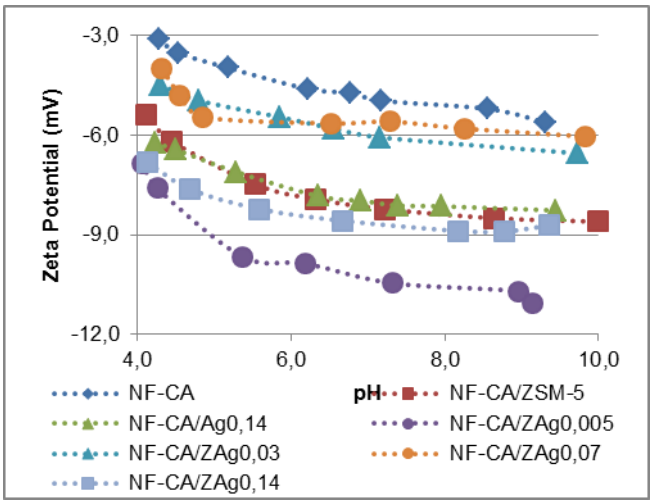

Figure 3-17 – Zeta potentials in the range of pH 4 – 9.

3.7 Evaluation of the bactericidal properties

In the first experiment with *P. aeruginosa*, the NFCA400-30, NFCA400-30ZSM5 and NFCA400-30Ag0,14 membranes revealed bacteriostatic effect (Figure 3-18), while NFCA400-30ZAg0,005, NFCA400-30ZAg0,03 and NFCA400-30ZAg0,07 membranes showed bactericidal effect (Figure 3-19) after 150 minutes. After 18 hours the membranes showed high bacterial growth.

Against *E. coli* and in the second experiment with *P. aeruginosa*, the membranes revealed absence of antibacterial effect after 250 minutes, with a visible growth. Against *P. aeruginosa* there was an increasing bacterial growth with the decreasing concentration of silver loaded zeolite. For both cultures, the NFCA400-30ZAg0,14 membrane showed the lowest bacterial growth after five hours. This result is expected since the membrane has the highest silver content (0,14%) trapped inside the ZSM-5 zeolite, which results in a gradual and more lasting release of silver ions [13]. The general absence of bactericidal effect may be related with the annealing process. Although incorporated particles, prepared *ex-situ*, are preferentially located in the skin layer of nanocomposite membranes during phase inversion process, which results in more accessible particles, the more intensive annealing treatment tightened the pores on the surface, which may have made the silver nanoparticles, zeolite and silver zeolite less accessible [29,37,38]. This assumption may be corroborated with the observed results after 18 hours, in which a decrease or a more controlled growth of *P. aeruginosa* was obtained for the membranes NFCA400-30Ag0,14, NFCA400-30ZAg0,07 and NFCA400-30ZAg0,14.

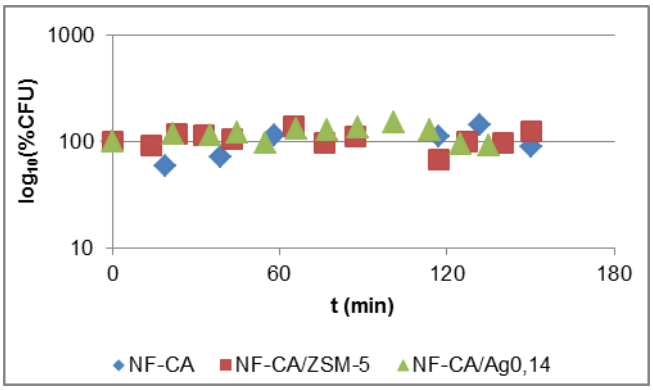

Figure 3-18 – Bactericidal effect of NFCA400-30, NFCA400-30ZSM5 and NFCA400-30Ag0,14 membranes against *P. aeruginosa* (1st).

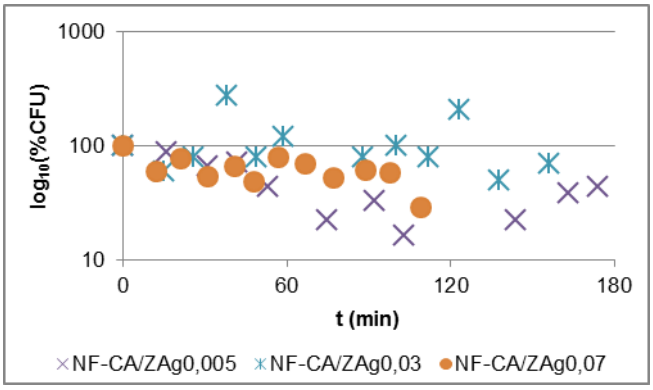

Figure 3-19 – Bactericidal effect of NFCA400-30ZAg0,005, NFCA400-30ZAg0,03 and NFCA400-30ZAg0,07 membranes against *P. aeruginosa* (1st).

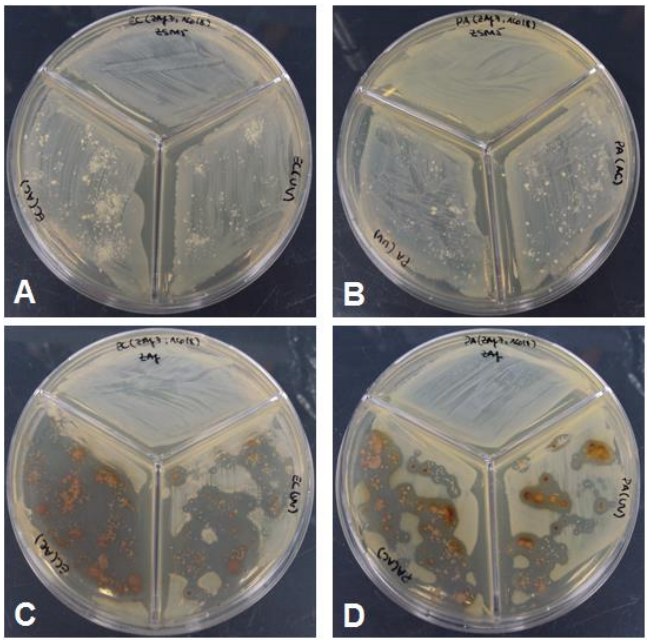

Figure 3-20 – Antibacterial effect of zeolite and silver zeolite: A) *E. coli* with ZSM-5 zeolite; B) *P. aeruginosa* with ZSM-5 zeolite; C) *E. coli* with ZAg; D) *P. aeruginosa* with ZAg.

The evaluation of the bacterial growth in the presence of the ZSM-5 zeolite/ZAg against *E. coli* and *P. aeruginosa*, comparing with the blank sample (Figure 3-20), leads to the conclusion that

ZSM-5 zeolite shows no antibacterial effect in both cultures, since there was no growth inhibition. The silver containing zeolite revealed a strong bactericidal effect for both cultures, being the effect more pronounced in *E. coli* than in *P. aeruginosa*. A change in the silver exchanged zeolite colour was observed after approximately 1,25 hours. Since it only occurred in the silver loaded zeolite, it can be stated that the colour change is due to the silver release from the zeolite to the agar medium, which may be due to the exchange between the silver inside the zeolite and the sodium present in the agar medium (15 g/L of tryptone, 5 g/L of papaic digest of soybean meal, 5g/L of sodium chloride and 15 g/L bacteriological agar).

4 CONCLUSIONS

Formamide reduces silver nitrate into silver particles of different sizes. It can be stated that a reducing agent, as sodium borohydride, is needed to obtain well-dispersed spherical silver nanoparticles. Hydraulic permeability and rejection coefficient is influenced by materials incorporation. Higher silver loaded zeolite concentrations in the membranes, although having the highest bactericidal effect, lead to a difficult cast of the membranes and decrease hydraulic permeability. The silver present in the zeolite in powder form and incorporated in the membrane is in the cationic form. The silver inside the zeolite seems to diffuse into more stable sites in the zeolite with time. Membranes have around 79% of non-structural water and small quantities of incorporated materials may not be homogeneously dispersed. The addition of materials to the membrane decreases zeta potential relatively to the cellulose acetate membrane. When sprinkled on bacteria, the ZSM-5 zeolite does not inhibit growth, while silver loaded zeolite shows higher bactericidal effect against *E. coli* than *P. aeruginosa*. The CA, CA/zeolite and CA/silver nanoparticles membranes revealed a bacteriostatic effect against *P. aeruginosa*, while the membranes with silver loaded zeolite showed bactericidal effect after 150 minutes. In a longer experiment, using *E. coli* and *P. aeruginosa*, the membranes revealed no antibacterial effect, which can be related with the less accessibility of the incorporated materials due to an annealing treatment with a higher temperature.

5 BIBLIOGRAPHY

[1] J. Wang, D.S. Dlamini, A.K. Mishra, M.M. Pendergast, M.C.Y. Wong, B.B. Mamba, V. Freger, A.R.D. Verliefde, E.M. V. Hoek, J. Memb. Sci. 454 (2014) 516–537.

[2] B. Van der Bruggen, M. Mänttäri, M. Nyström, Sep. Purif. Technol. 63 (2008) 251–263.

[3] M.R. Wiesner, S. Chellam, Environ. Sci. Technol. 33 (1999) 360–366.

[4] H. Xie, T. Saito, M.A. Hickner, Langmuir 27 (2011) 4721–4727.

[5] M.M. Pendergast, E.M. V. Hoek, Energy Environ. Sci. 4 (2011) 1946–1971.

[6] P. Rauwel, E. Rauwel, S. Ferdov, M.P. Singh, 2015 (2015) 2–4.

[7] C. Caro, P.M. Castillo, R. Klippstein, D. Pozo, A.P. Zaderenko, Silver Nanoparticles, InTech, 2010.

[8] M. Rai, A. Yadav, A. Gade, Biotechnol. Adv. 27 (2009) 76–83.

[9] B. Le Ouay, F. Stellacci, Nano Today 10 (2015) 339–354.

[10] D.Y. Koseoglu-Imer, B. Kose, M. Altinbas, I. Koyuncu, J. Memb. Sci. 428 (2013) 620–628.

[11] P. Lalueza, M. Monzón, M. Arruebo, J. Santamaría, Mater. Res. Bull. 46 (2011) 2070–2076.

[12] L. Ferreira, A.M. Fonseca, G. Botelho, C.A. Aguiar, I.C. Neves, Microporous Mesoporous Mater. 160 (2012) 126–132.

[13] T. Matsuura, Y. Abe, Y. Sato, K. Okamoto, M. Ueshige, Y. Akagawa, J. Dent. 25 (1997) 373–377.

[14] D.L. Boschetto, L. Lerin, R. Cansian, S.B.C. Pergher, M. Di Luccio, Chem. Eng. J. 204–205 (2012) 210–216.

[15] A.S. Figueiredo, M.G. Sánchez-Loredo, A. Maurício, M.F.C. Pereira, M. Minhalma, M.N. de Pinho, J. Appl. Polym. Sci. 132 (2015).

[16] H. Wang, X. Qiao, J. Chen, X. Wang, S. Ding, Mater. Chem. Phys. 94 (2005) 449–453.

[17] U. of Canterbury, (2015) 1–2.

[18] M.N. De Pinho, Desalination 68 (1988) 211–221.

[19] M.D. Afonso, M.N. De Pinho, Desalination 79 (1990) 115–124.

[20] M.J. Rosa, M.N. De Pinho, J. Memb. Sci. 89 (1994) 235–243.

[21] M.D. Afonso, M.N. De Pinho, J. Memb. Sci. 179 (2000) 137–154.

[22] W.E.F. American Public Health Association, American Water Works Association, Standard Methods for the Examination of Water and Wastewater, 1999.

[23] S. Corporation, Total Organic Carbon Analyzer TOC-VCPH/CPN, 2009.

[24] M.A.N.D.A. Lemos, P. Sousa, F. Lemos, A.J.L. Pombeiro, F. Ramôa Ribeiro, Stud. Surf. Sci. Catal. 122 (1999) 443–446.

[25] P.E. Inc., A Beginner's Guide to Thermogravimetric Analysis, 2004.

[26] S. Bhattacharjee, J. Control. Release 235 (2016) 337–351.

[27] F. Thielbeer, K. Donaldson, M. Bradley, Bioconjug. Chem. 22 (2011) 144–150.

[28] A.P. GmbH, EKA: Electro Kinetic Analyzer Instruction Manual, Austria, 2003.

[29] M. Sile-Yuksel, B. Tas, D.Y. Koseoglu-Imer, I. Koyuncu, Desalination 347 (2014) 120–130.

[30] J. Caro, M. Bülow, W. Schirmer, J. Chem. Soc. Faraday Trans. 1 81 (1985) 2541–2550.

[31] R. Desai, V. Mankad, S.K. Gupta, P.K. Jha, Int. J. Nanosci. 4 (2012) 30–34.

[32] A. Zielińska, E. Skwarek, A. Zaleska, M. Gazda, J. Hupka, Procedia Chem. 1 (2009) 1560–1566.

[33] L. Baia, S. Simon, Mod. Res. Educ. Top. Microsc. (2007) 576–583.

[34] J. Widoniak, S. Eiden-Assmann, G. Maret, Colloids Surfaces A Physicochem. Eng. Asp. 270–271 (2005) 340–344.

[35] Y.-J. Li, C.-Y. Liu, J. Electroanal. Chem. 517 (2001) 117–120.

[36] J.O. Abitoye, P. Mukherjee, K. Jones, Environ. Sci. Technol. 39 (2005) 6487–6493.

[37] J.S. Taurozzi, H. Arul, V.Z. Bosak, A.F. Burban, T.C. Voice, M.L. Bruening, V. V. Tarabara, J. Memb. Sci. 325 (2008) 58–68.

[38] D. Murphy, M.N. de Pinho, J. Memb. Sci. 106 (1995) 245–257.